Title

Incorporating Carbon Nanotube Sheets into Carbon Fiber Reinforced Polymer Tubes for Space Support Structure

Author

Soemardy, Ebryanto

Publication Date

2024

Peer reviewed|Thesis/dissertation

UNIVERSITY OF CALIFORNIA

Los Angeles

Incorporating Carbon Nanotube Sheets into Carbon Fiber Reinforced Polymer Tubes for Space Support Structure

A thesis submitted in partial satisfaction of the requirements for the degree Master of Science in Mechanical Engineering

by

Ebryanto Soemardy

2024

ABSTRACT OF THE THESIS

Incorporating Carbon Nanotube Sheets into

Carbon Fiber Reinforced Polymer Tubes for

Space Support Structure

by

Ebryanto Soemardy

Master of Science in Mechanical Engineering

University of California, Los Angeles, 2024

Professor Xiaochun Li, Chair

Carbon fiber reinforced polymer (CFRP) is widely used in space support structures for its exceptional mechanical properties, yet its weakness in the transverse direction due to resin matrix limitations remains a significant challenge [1,19]. This study investigates the effectiveness of incorporating carbon nanotube (CNT) sheets to enhance the flexural strength of thin-walled unidirectional CFRP tubes. Results demonstrate a remarkable 115% increase in flexural strength compared to tubes composed solely of unidirectional carbon fiber, highlighting the potential of CNT sheets in mitigating delamination and improving mechanical performance.

However, analysis of the fiber volume fraction (FVF) reveals a lower-than-expected value of approximately 40%, attributed to significant resin trapping between

layers. This finding underscores the need for alternative manufacturing methods, such as pultrusion, to address resin entrapment and improve FVF.

These findings have important implications for the design and fabrication of CFRP structures in aerospace applications. Future research efforts will focus on optimizing manufacturing techniques to enhance FVF and further improve the mechanical properties of CFRP tubes.

The thesis of Ebryanto Soemardy is approved.

Gregory P. Carman

Jonathan Hopkins

Xiaochun Li, Committee Chair

University of California, Los Angeles

2024

Tables and Figures

Acknowledgements

I would like to thank Professor Xiaochun Li for welcoming me and giving me the opportunity to perform research in his lab. I have learned an incredible amount from Professor Li during my master's studies, from academics to life lessons. I greatly appreciate his wisdom and inspiration for making scientific discoveries.

I would also like to thank the members of my committee (Professor Xiaochun Li, Professor Gregory Carman, and Professor Jonathan Hopkins) for taking time out of their busy schedule to review my thesis at a moment's notice.

I would also like to thank Larry Carlson for allowing me to perform research in his lab and serving as a mentor for this research. Larry was a guiding force that provided me with new ideas whenever I got stuck during this study.

Finally, I would like to thank the members of the Scifacturing lab for welcoming and guiding me, as well as providing a familial atmosphere in the lab, allowing me to enjoy my time doing research alongside them. Special thanks to Alex Killips for working directly alongside me on this project.

I. Introduction/Motivation

The demand for reliable lightweight designs continues to rise, particularly in aerospace applications as an endeavor to use less or lower density materials that can produce similar or even enhanced technical performance [8]. As such, typical structures in the field are constructed from composites rather than metals. Numerous studies have shown the exceptional potential of carbon fiber-reinforced polymer (CFRP) as one of the most promising candidates for stable space structures owing to its low mass, high stiffness, and superior thermal stability [1,2]. CFRP is used extensively on satellites and payload support structures [3]. However, challenges emerge when these support structures incur damage, requiring repair or replacement. Current conventional approach involves crafting a new support structure on Earth to be sent out to space as payload, where astronauts then receive the package and replace the damaged structures. This process is extremely expensive and inefficient due to the limited space within the payload, especially concerning large structures such as solar arrays, antennas, and optical systems.

To address this problem, DARPA initiated a project called Novel Orbital and Moon Manufacturing, Materials, and Mass-efficient Design (NOM4D). The purpose of this project is to develop the foundations of building robust, precise structures in space rather than on Earth. This way, only raw materials would need to be ferried from Earth to orbital construction facilities, where they would be processed and used for manufacturing. Finished structures can then be used directly in orbital applications, thus eliminating most prevailing launch constraints.

This thesis explores various materials and configurations of carbon fiber lay-ups to fabricate tubular CFRP with high stiffness and high fiber volume fraction with DCPD. Additionally, it aims to maintain the total mass loss of all materials below 1%, which aligns with NASA's maximum allowed mass loss for materials in space.

II. Literature Review

Section 2.1 Dicyclopentadiene Resin

Dicyclopentadiene (DCPD) is a monomer that is a clear and colorless liquid with low viscosity, commercially derived from petrochemicals. DCPD can be polymerized into poly-dicyclopentadiene (poly-DCPD) by undergoing a process called ring-opening metathesis polymerization (ROMP). [7] Like other ROMP polymers, poly-DCPD has excellent toughness that usually fails in a ductile rather than brittle manner. It displays "high resistance to chemicals and water absorption while exhibiting an inherent toughness that is usually not associated with thermoset polymers". [6]

Section 2.1.1 Ring-Opening Metathesis Polymerization Process

ROMP is a chain growth polymerization process where cyclic olefins are converted into linear polymers that contain olefins in the main chain [9]. Simply put, cyclic olefins form a linear structure with double bonds in the backbone as shown in figure 2.1.1.1.

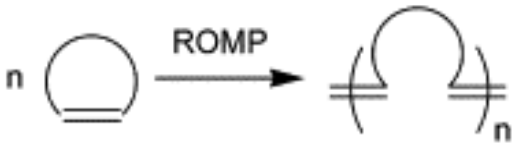

Figure 2.1.1.1 Generalized example of ROMP reaction [9].

The polymerization mechanism of ROMP can be broken down into three main steps: initiation, propagation, and termination, displayed in figure 2.1.1.2. The initiation step begins with the coordination of a metal alkylidene complex to a cyclic olefin that subsequently goes through [2+2] cycloaddition, producing a four-membered

metallacyclobutane intermediate to form the beginning of a growing polymer chain. The intermediate then goes through cycloreversion to afford a new metal alkylidene. At this point the resulting complex has gotten larger, but the reactivity towards cyclic olefins remains similar, allowing the previous steps to be repeated to lengthen the polymer chain during the propagation stage. Once the monomer is completely consumed, the reaction enters the termination stage where addition of ethyl vinyl ether is commonly used to quench the ROMP process. The ethyl vinyl ether reacts with the metal carbene species in a growing chain end and removes the metal from the polymer, prohibiting the chain from growing further. [9,10]

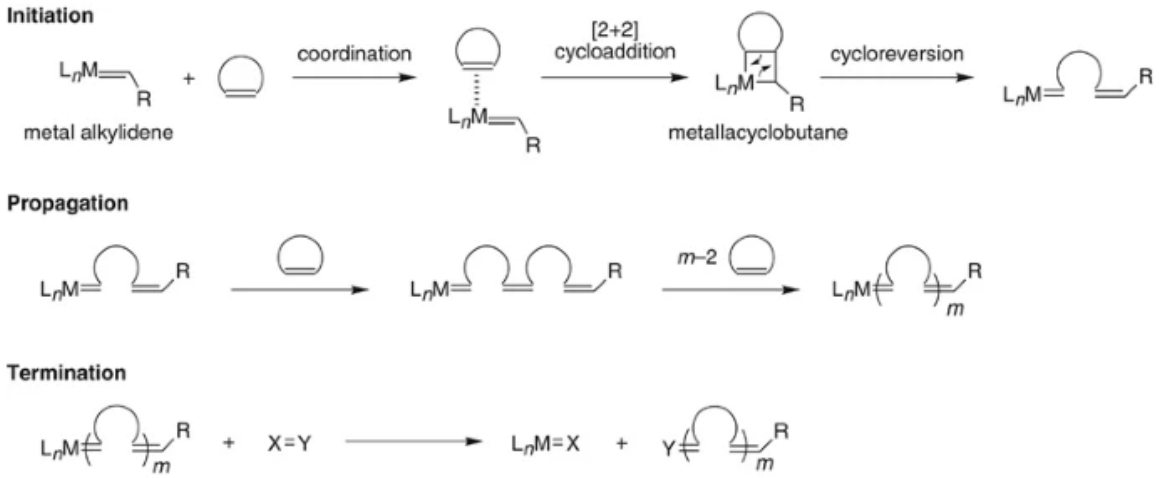

Figure 2.1.1.2 The three steps of the mechanism of ROMP [10].

Problems arise when chain transfer occurs during the ROMP process, causing an interconversion of the polymer chain increasing the polydispersity indices (PDI). Figure 2.1.1.3 shows two common types of chain transfers that can manifest during ROMP: intermolecular and intramolecular. In the intermolecular chain transfer, a

polymer chain with an active metal alkylidene on its end reacts with a double bond in another chain, causing a transfer in molecular weight between the two chains. In the intramolecular chain transfer, the carbene end of a chain reacts with itself to form another polymer chain with lower molecular weight and a cyclic oligomer. Both of these processes result in the increase of the PDI of the polymer product, which would ideally be minimized. [10]

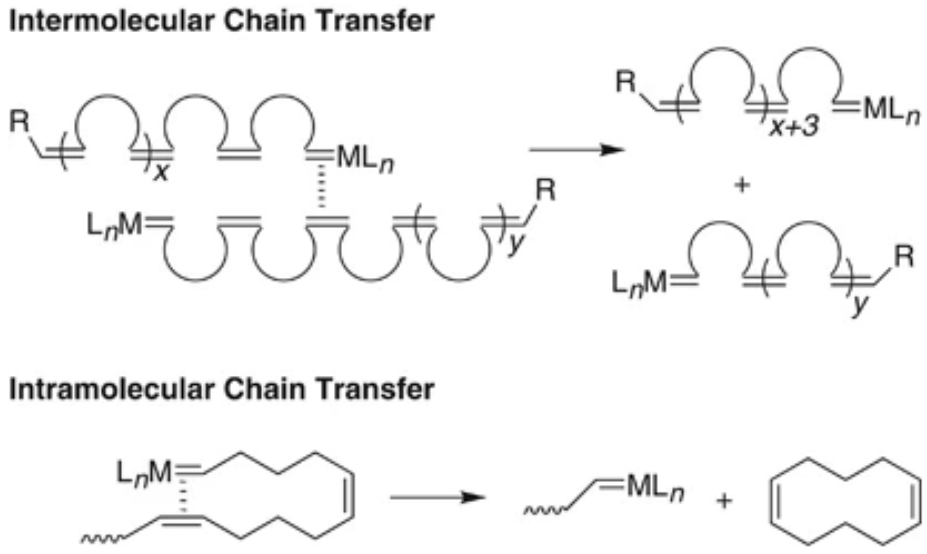

Figure 2.1.1.3 Chain transfer reactions in ROMP [10].

The solution to avoiding these undesired chain transfers lies in the selection of the catalyst. The catalysts are typically complexes of transition metals with ligands that can be selected to tune its specificity. This allows the catalyst to react with specific double bonds within the system, thus discouraging chain transfer processes. [10]

Section 2.1.2 DCPD Catalyst

Different transition-metal-based metathesis catalysts have been used to activate the ROMP process of DCPD, each resulting in very different molecular structure

of the produced polymers. Therefore, catalyst plays a significant role in the physical and chemical properties of the final material formed. DCPD contains two olefins, norbornene and cyclopentene, both of which have the capabilities to bind to the catalyst and undergo metathesis. However, the ring strain of the norbornene olefin is higher than that of the cyclopentene, causing norbornene to bind to the catalyst and leading to metathesis more frequently. As a result, the cyclopentene olefin undergoes little to no polymerization until after the norbornene olefin is depleted, further leading to the production of cross-linked polymer as displayed in figure 2.1.2.1. [7]

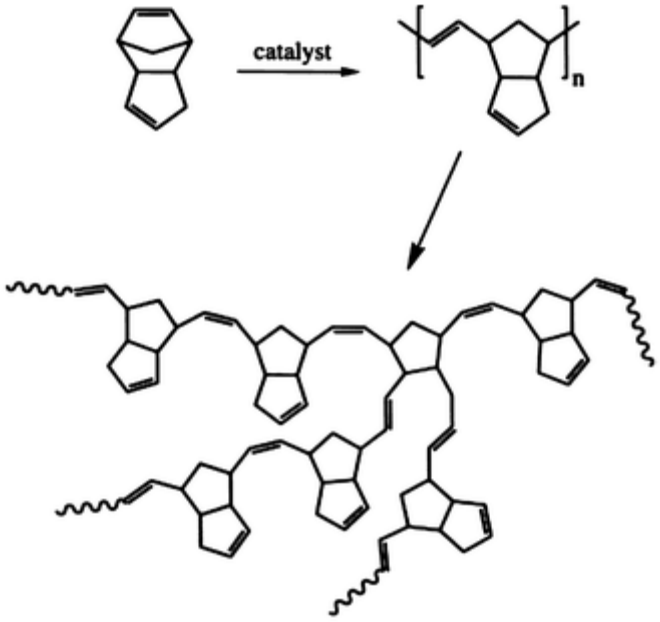

Figure 2.1.2.1 ROMP reaction scheme for endo-DCPD [7].

Yang et al. compared the curing kinetics and mechanical properties of endo-DPCD that are synthesized using first- and second-generation Grubbs' catalysts displayed in figure 2.1.2.2. This work studies the isothermal curing kinetics of endo-DCPD using first- and second-generation Grubbs' catalyst at four different temperatures

as well as a subsequent dynamic measurement to determine the residual reaction enthalpy using differential scanning calorimetry (DSC). Additionally, dog-bone-shaped cured samples were also prepared in a brass mold for each Grubbs' catalyst system for tensile testing.

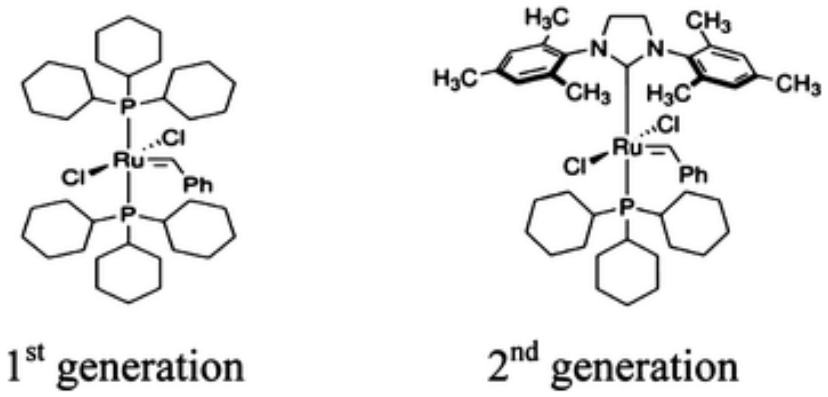

Figure 2.1.2.2 First- and second-generation Grubbs' Catalyst [7].

The DSC from the isothermal curing showed very different curves between the first- and second-generations Grubbs' catalyst systems as shown in figure 2.1.2.3. The DSC from the second-generation Grubbs' catalyst system comprise of an exothermic peak and a large maximum heat flow value, implying a significantly faster overall ROMP reaction of endo-DCPD. On the other hand, the dynamic DSC scans were very similar for both Grubbs' catalyst systems, resulting in similar residual reaction enthalpy. [7]

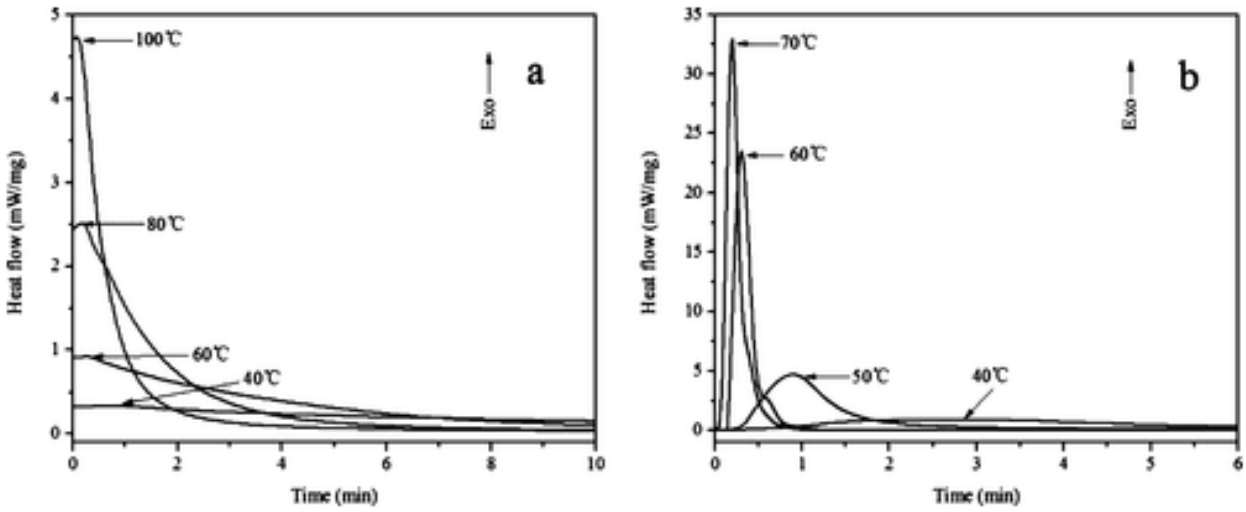

Figure 2.1.2.3 Isothermal DSC scans of endo-DCPD with (a) first- and (b) second-generation Grubbs' catalyst. [7]

The tensile tests produced the stress-strain curve in figure 2.1.2.4, showing that samples of both Grubbs' catalyst systems exhibit plastic deformation. In both samples the tensile stress increases sharply up to the yield point before necking with local diminution in dimension in the gauge region of the sample, followed by another slight increase until fracture. Table 2.1.2.1 shows that the second-generation Grubbs' catalyst system produces slightly lower Young's modulus and yield strength, but a significantly higher toughness compared to that of the first-generation Grubbs' catalyst system. [7]

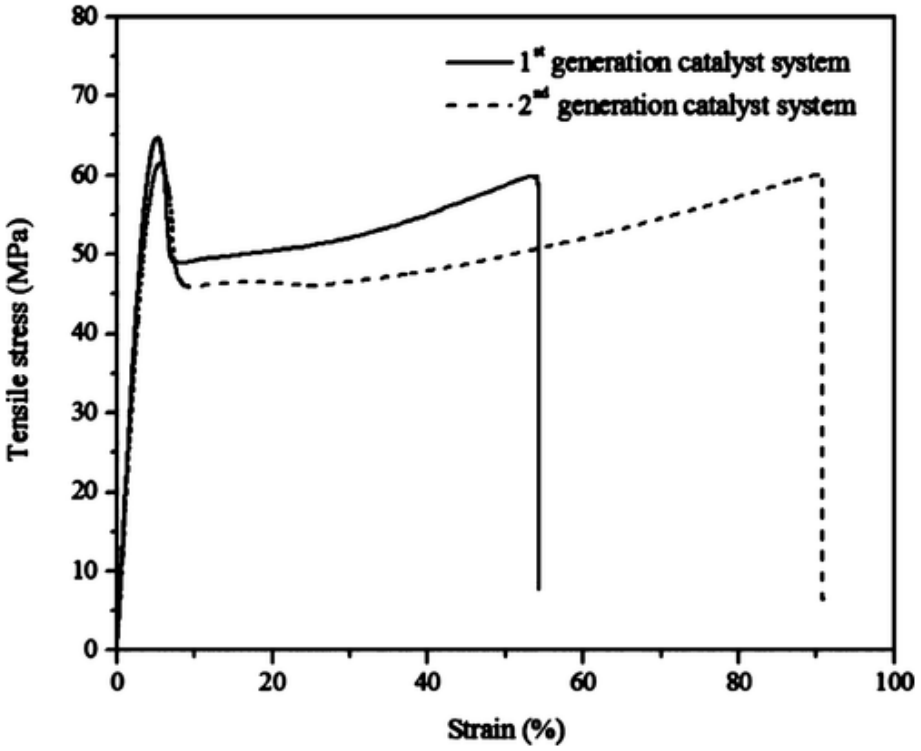

Figure 2.1.2.4 Stress-strain curves for poly-DCPD initiated by first- and second-generation Grubbs' catalyst. [7]

Table 2.1.2.1 Tensile tests results for poly-DCPD with first- and second-generation Grubbs' catalyst. [7]

	E (GPa)	σ_y (MPa)	ε_f (%)	Toughness (MPa)
1st Generation Catalyst	1.838 ± 0.07	64.75 ± 1.64	54.22 ± 2.64	28.27 ± 4.42
2nd Generation Catalyst	1.713 ± 0.04	61.49 ± 1.34	90.76 ± 5.30	45.61 ± 4.90

Yang et al. has shown that poly-DCPD initiated by second-generation Grubbs' catalyst is superior in both curing kinetics and mechanical properties compared to poly-DCPD initiated by first-generation Grubbs' catalyst. Even though it produces poly-DCPD with slightly lower Young's modulus and yield strength, it has a much faster curing rate and a substantially higher toughness. [7]

Section 2.1.3 Frontal Ring-opening Metathesis Polymerization

A major advantage of using DCPD is its ability to sustain frontal ring-opening metathesis polymerization (FROMP) shown in figure 2.1.3.1, which entails a reaction that is highly exothermic and reacts quickly at the adiabatic reaction temperature but slowly at ambient temperature [12]. Frontal polymerization is initiated by a local thermal stimulus that kickstarts a propagating front that rapidly polymerizes available monomers [11]. Compared to traditional polymerization methods, FROMP is superior in various fields, including simpler operating processes, faster reaction rate, better homogeneity, higher energy and material efficiency [13].

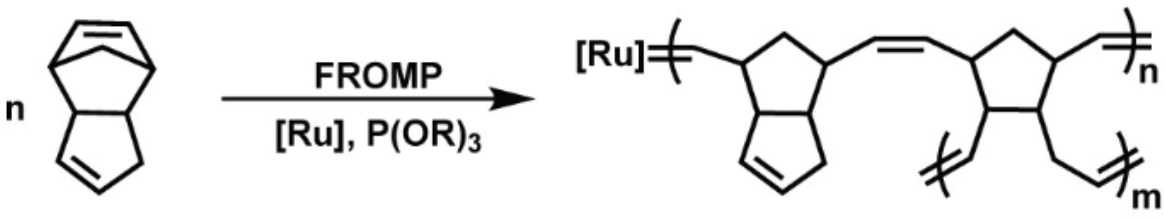

Figure 2.1.3.1 Chemical reaction of DCPD through FROMP [11].

A major challenge of utilizing FROMP is its tendency to polymerize before frontal initiation, also known as spontaneous polymerization (SP). This problem is especially significant since frontal polymerization relies on minimal reactivity at working temperature and high activity at initiation temperature, producing a high frontal velocity and long pot-life. Low pot-life is usually caused by the propagating catalyst species, producing a viscous mixture and a rise in temperature that rapidly polymerizes monomers. To combat this, inhibiting agents are required to be mixed into the monomers before adding catalyst to extend its pot-life. [11]

Robertson et al. has demonstrated that using alkyl phosphites as inhibitors can improve the pot-life of DCPD/second-generation Grubbs' catalyst solutions, while maintaining FROMP capability to form fully cured poly-DCPD. Figure 2.1.3.2 shows the phosphite-inhibited FROMP reaction inside a small test tube and its general mechanism. [15]

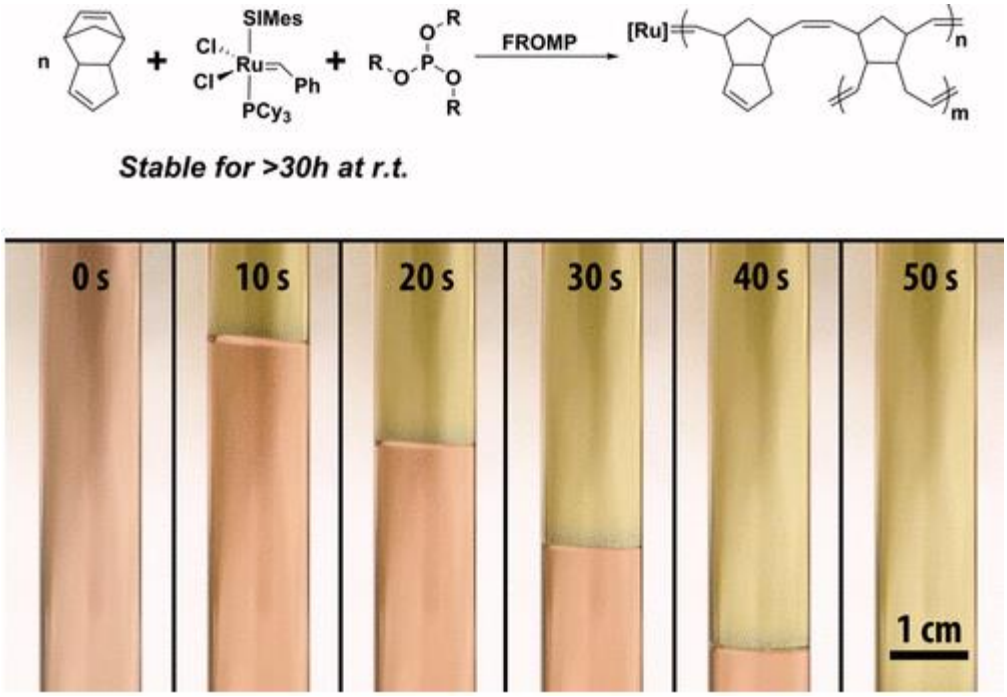

Figure 2.1.3.2 Scheme for phosphite-inhibited FROMP reaction [15].

In this study, trimethyl phosphite (TMP), triethyl phosphite (TEP), and tributyl phosphite (TBP) are tested as inhibitors for FROMP reaction of DCPD at a range of concentrations to explore the effects on frontal velocity and pot life. The results are shown in figure 2.1.3.3 and figure 2.1.3.4. This work successfully demonstrated that all the tested phosphite groups were able to control the pot-life in the range of 1 to 30 hours simply by varying the inhibitor concentration, with TBP being the most effective. A 1:1 inhibitor:catalyst concentration of TBP is able to increase the pot-life to over 5

hours. The frontal velocity, on the other hand, shows an inverse trend to the pot life and phosphite concentration. Equal parts of inhibitor and catalyst reduced the frontal velocity of DCPD by about 40%. There were no significant differences in the effect of the three phosphites on the frontal velocity. [15]

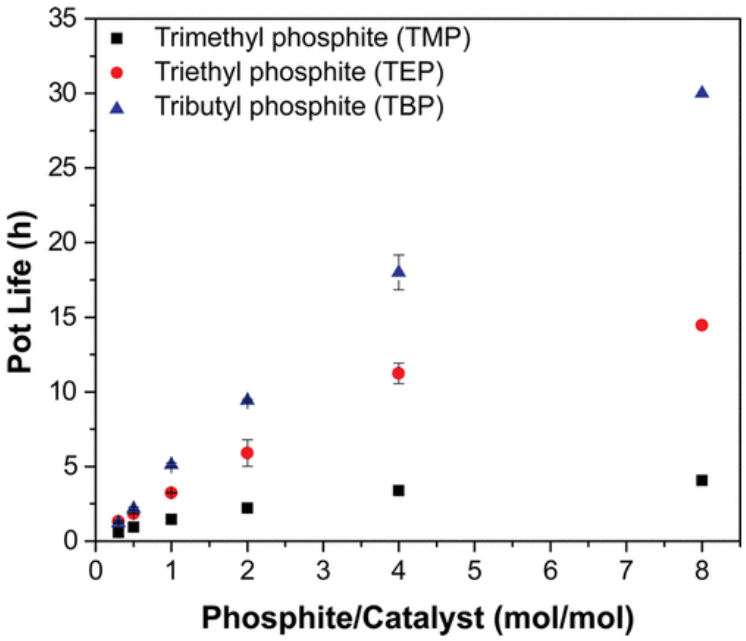

Figure 2.1.3.3 Effect of alkyl phosphite inhibitors on pot-life of FROMP solutions [15].

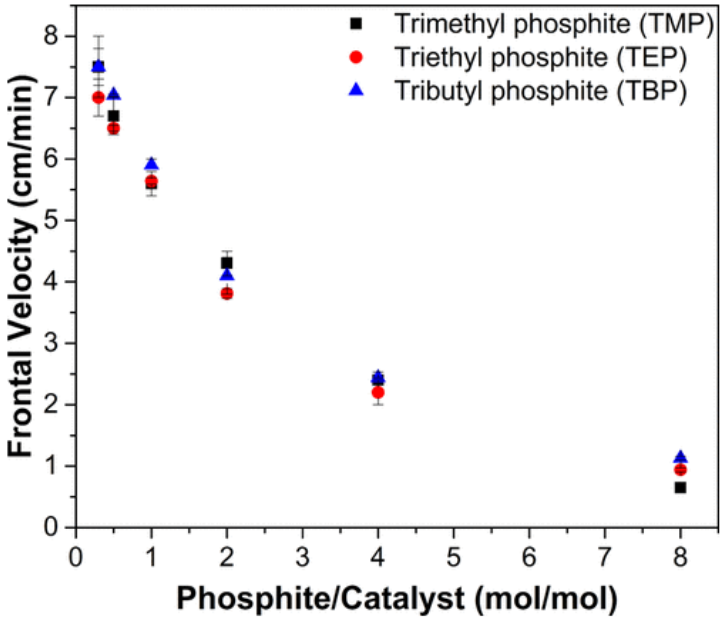

Figure 2.1.3.4 Effect of alkyl phosphite inhibitors on frontal velocity of FROMP solutions [15].

Section 2.2 CFRP Delamination

Although unidirectional carbon fiber reinforced polymer composites have excellent strength and modulus along the continuous fiber direction, the lack of reinforcement in the transverse direction can lead to premature failure in the form of delamination [5]. In a CFRP laminate, the bearing and bonding between layers of laminates are only supported by the resin matrix, leading to low fracture toughness in the thickness direction. Furthermore, the difference in Poisson's ratio and thermal expansion coefficient between the fiber and the resin matrix heavily contributes to the mismatch of inter-ply stiffness and increased interlaminar stress concentration. The combination of these factors has been known to be the reason CFRP laminates to delaminate under little load or impacted by low energy [19]. Zhu et al. has found that toughening the interlaminar interface is an effective way to combat delamination [22].

Previous attempts that successfully reduced delamination included various stitching and Z-pinning techniques. Although effective, these methods have been observed to significantly alter the alignments of the continuous carbon fiber, leading to reduction in both strength and stiffness. Instead, providing inter-fiber reinforcement carbon nanotubes (CNT) has been shown to be much more effective. [5]

Section 2.3 Properties of Carbon Nanotubes

CNTs are "sp^2 nanocarbon materials with tubular structures composed of rolled-up graphene sheets", exhibiting tensile strength much higher than that of steel, thermal conductivity better than that of diamond, very low weight and density, and extremely high aspect ratio. The main types of CNTs are classified as single-walled

carbon nanotubes (SWCNTs) and multi-walled carbon nanotubes (MWCNTs) shown in figure 2.3.1, where MWCNTs are typically stronger but more rigid while SWCNTs are weaker, but much more flexible to allow deformations. [18,24]

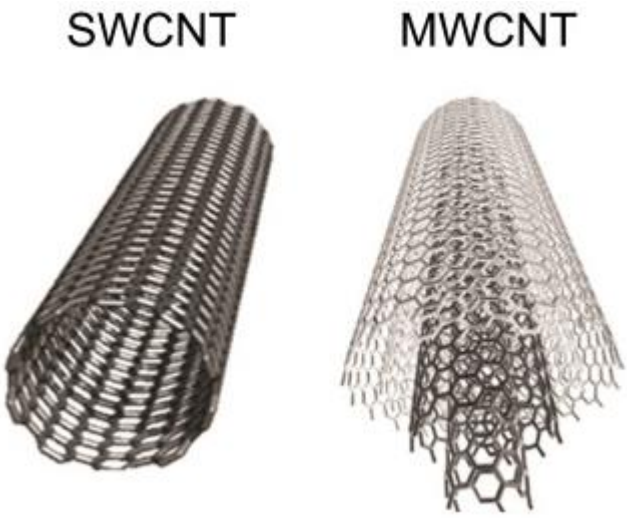

Figure 2.3.1 Schematic illustrations of SWCNT and MWCNT [24].

Under tensile load, CNT exhibits a double pentagon-heptagon (5-7-7-5) dislocation, leading to either a plastic yield or a brittle fracture [25]. In the case of the plastic yield, the (5-7-7-5) dislocation loop "ease further relaxation by separating the two dislocation cores", which glides along the helical path of the CNT [18]. This corresponds to a plastic flow and results in a significant reduction in diameter and chirality of the CNT, while giving rise to ductile behavior [24]. In the case of the brittle fracture, SWCNT can only exhibit the complete fracture of nanotube walls, due to its single-walled nature. MWCNT, on the other hand, can sometimes present a sword-in-sheath failure mode depicted in figure 2.3.2. This fracture morphology occurs when defects occur in different planes between the inner and outer layers of MWCNT, producing a sum of fractured fragment lengths that far exceed the original section

length. This phenomenon can be explained by weak van der Waals binding forces between the shells after breakage of the outermost shell occurs. [26]

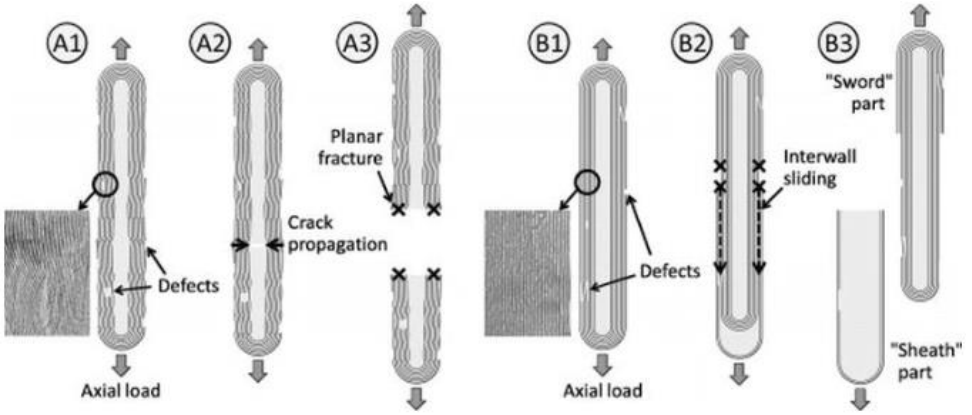

Figure 2.3.2 Examples of (A1-A3) complete fracture type failure and (B1-B3) sword-in-sheath type failure in CNT [26].

Unlike the high rigidity and high strength along the axial direction, CNT is relatively compressible and deformable in the transversal direction. That being said, CNT is also extremely elastic and resilient, shown in a previous study that proved a large force exerted on CNT produced a reversible and elastic deformation, leading to the conclusion that "radial mechanical force may not be capable of cutting a nanotube". However, a buckling pattern in CNT was then observed in another study, indicating that there exists a critical diameter at a given load and CNT length for the possibility of a rippling mode. This is further proven with the observation of a fully collapsed MWCNTs after compressive loading. Sharma et al. reported that the lattice symmetry of SWCNT bundle was preserved up to a pressure of 13 GPa applied quasi-hydrostatically. In addition, Yu et al. quantified the deformability of MWCNT by an indentation force,

producing an effective elastic modulus in the range of 0.3 to 4 GPa with the ability to reversibly deform up to a strain of 50%. [25]

Yu et al. also conducted an experimental study of the fundamental mechanical properties of CNT, including its Young's modulus, tensile, and shear strength. To perform tensile testing, both MWCNT and SWCNT in the form of nano-ropes are attached to AFM probes shown in figure 2.3.3. The nanotubes are then stretched along the tensile direction by one of the AFM probes. Figure 2.3.4 and figure 2.3.5 show the stress-strain curve of the MWCNT and SWCNT tensile tests, respectively. The Resulting Young's modulus value of the MWCNT were in the range of 270 to 950 GPa, with an assigned effective thickness of 0.34 nm, while that of the SWCNT were in the range of 320 to 1470 GPa. The tensile strength of MWCNTs was measured to be in the range of 11-63 GPa with the strain reaching up to 12% at the breaking point. The failure of the MWCNTs in this test was observed to be a sword-in-sheet type failure. On the other hand, the tensile strength of SWCNTs was measured to be within the range of 13-52 GPa, with a strain of 5.3% or lower at the breaking point. [25]

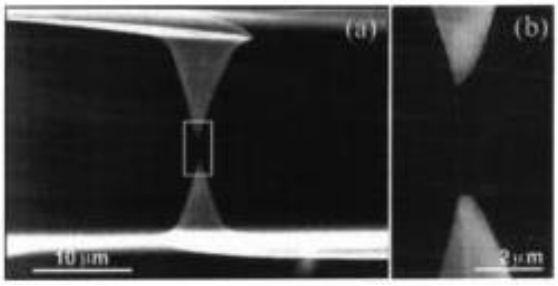

Figure 2.3.3 Carbon nanotube mounted between two atomic force microscope (AFM) probes [25].

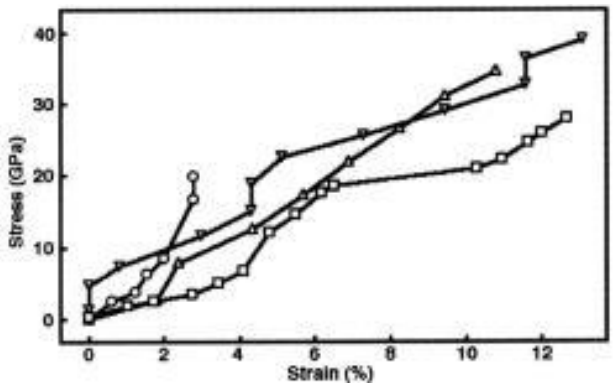

Figure 2.3.4 Stress-strain curve for measured MWCNT [25].

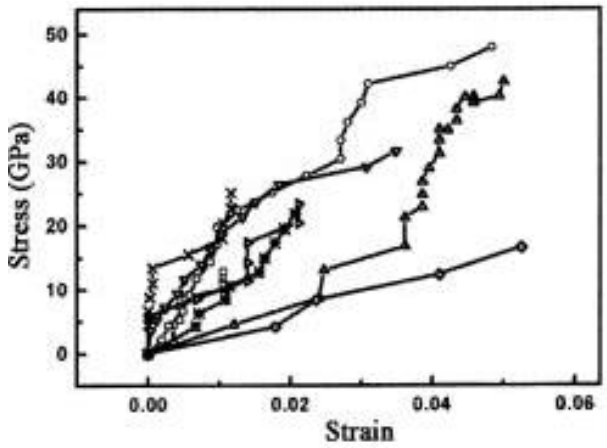

Figure 2.3.5 Stress-strain curve for measured SWCNT [25].

These values are on the lower end, compared to other studies that have been done. Oleg et al. had performed a tensile test of a small strand of SWCNT ropes using a MEMS strain stage inside a transmission electron microscope, obtaining tensile strength of about 140 GPa. Additionally, Demczyk et al. measured the tensile strength of MWCNT using the same method to be about 150 GPa, while obtaining a similar Young's modulus value. [25]

MWCNT structure consists of nested cylinders of rolled graphene sheet, which provides an opportunity for the study of the weak van der Waals interaction between atomic perfect surfaces. With a gap of about 0.34 nm, it is expected that there is little

for the relative sliding between nested layers, allowing the pull-out of the inner shells as shown in figure 2.3.6. Yu et al. suggests that the forces responsible for the sliding resistance includes surface tension, shear elastic force, and edge effect force. The sliding resistance force can be described as $\mathrm{F}_a = \mathrm{F}_s + \mathrm{F}_i = \pi \mathrm{d} \tau \mathrm{L}(\mathrm{t}) + \mathrm{F}_i$, where F_a is the applied pulling force, τ is the shear strength, *L* is the contact length, *d* is the shell diameter, and F_i are forces from surface tension and edge effects. They also measured the shear strength for a smooth pull out and a stick-slip type sliding, producing a shear strength of 0.08 MPa and 0.3 MPa, respectively. This difference can be explained by the different degree of interlayer interaction between the sliding types. [25]

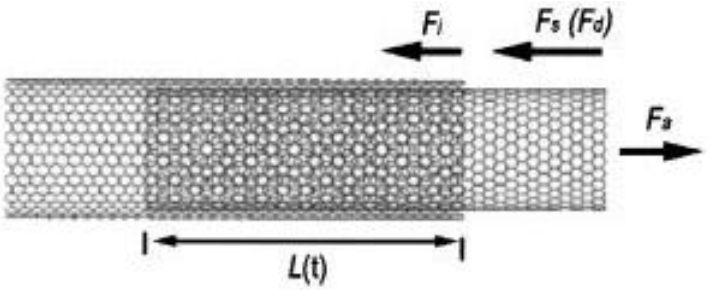

Figure 2.3.6 Schematic of interlayer sliding in MWCNT [25].

Section 2.3.1 CNT Reinforced CFRP

The biggest advantage of CNT-reinforced CFRP is the realization of three modification methods: modifying bulk matrix, modifying fibers, and reinforcing the interlaminar interface. These modifications ultimately enhance the mechanical properties of the CFRP through two coexisting enhancement mechanisms: chemical bonding and mechanical interlocking. Chemical bonding is controlled by surface wetting and occurs when chemical connection is formed at the interface only after the chemical reaction between the matrix and reinforcement has taken place. On the other hand,

mechanical interlocking occurs when connection between reinforcement and the matrix is caused by micro rough structure of the surface. This mechanism is controlled by surface roughness of the reinforcement and the shrinkage of the matrix. Mechanical locking may be the dominating strengthening mechanism, but it will always be accompanied by a weak van der Waals force between the matrix and the reinforcement as well as chemical bonding. [19]

Saadatyar et al. experimentally quantified the mechanical properties of MWCNT-reinforced unidirectional carbon fiber-reinforced epoxy in both transverse and longitudinal fiber directions. The tensile test was carried out in the transverse fiber direction, producing the stress-strain curve in figure 2.3.1.1. The results indicated that the addition of 0.1 phr MWCNT increased the tensile strength by 28.5%, modulus by 25%, and break strain by 14%. These enhancements are attributed to MWCNTs in the matrix reducing and delaying the growth of cracks in the sample and the improved adhesion between fibers and matrix. Higher concentration of MWCNT seemed to worsen the mechanical properties because of their agglomeration from their strong van der Waals interaction. Oversaturation of MWCNT seemed to also cause increased viscosity in the resin, leading to reduced wettability and consequently decreased adhesion between fiber and resin. [19]

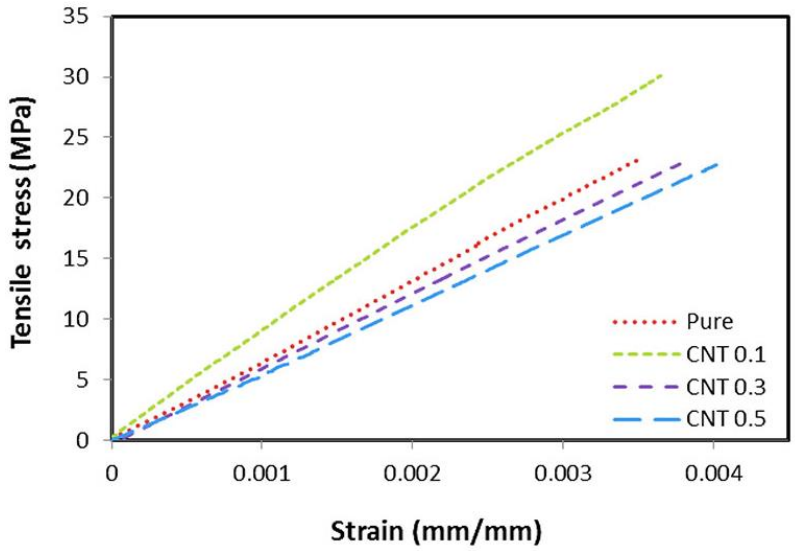

Figure 2.3.1.1 Tensile stress-strain curves of CFRE with different amounts of MWCNT [19].

The flexural test was carried out in the longitudinal fiber direction, producing the stress-strain curve in figure 2.3.1.2. The results showed that addition of 0.1 phr MWCNT resulted in an increase of 5% in flexural without changing the modulus. The presence of MWCNT also increased the deflection at break of the samples by about 13%. Compared to the enhancements in the transverse fiber direction, the longitudinal fiber direction didn't get much improvement from the addition of MWCNT. This lack of increase in flexural strength is due to the test being executed in the longitudinal direction where mechanical properties are dominated by the fibers. Additionally, the load bearing of the MWCNT-reinforced epoxy is negligible compared to the high strength of the fiber in that direction, affecting the flexural properties minimally. Like the tensile tests, samples with heavier concentration of MWCNT have weakened flexural properties due to nanoparticle agglomeration. [19]

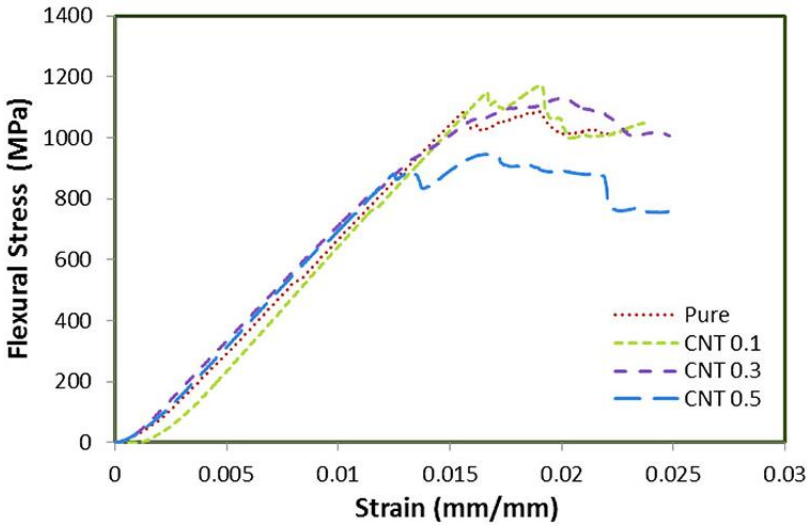

Figure 2.3.1.2 Flexural stress-strain curves of CFRE with different amounts of MWCNT [19].

The fracture toughness test was carried out in both transverse and longitudinal directions of the fibers to indicate the resistance of the composite against damage and crack growth. The addition of 0.3 phr of MWCNT resulted in an increase of 39% in the fracture toughness along the transverse direction, attributable to the prevention of rapid crack growth provided by MWCNTs. The nanoparticles are thought to cause crack deviations in the matrix, requiring more cracks to induce fracture and effectively delaying it. High concentration of MWCNT fails to improve the fracture toughness due to the same nanoparticle agglomeration discussed before. Like the flexural strength, incorporation of MWCNT did not change the fracture toughness in the longitudinal direction of the fibers since the property was dominated by the fibers. [19]

This study successfully demonstrated that incorporating a small amount of CNT into CFRP can significantly enhance its mechanical properties in the transverse direction of the fibers. The longitudinal direction, on the other hand, did not improve much due to the strength unidirectional fibers intrinsically have in that orientation.

Section 2.3.2 CNT Sheet Interleave

Interleaving is a common technique in the aerospace industry, used to improve acoustic damping and discouraging crack propagation in metallic structures. Recently, studies have emerged showing interest in using CNT veils/sheets as interleaves in layered CFRP in an attempt to produce similar effects. Interleaving CNT sheets have been proven to generate some toughening mechanisms, including carbon fiber bridging and matrix level CNT bridging, both of which lead to a rising R-curve. In addition, crack propagation in the CFRP showed regular crossings between interlayers. This behavior triggers produces a failure mode that combines CNT and carbon fiber pullout, as well as debonding between fiber and resin matrix, thus enhancing interlaminar toughness. However, when densified CNT veils are interleaved the fracture surface shows peeling of CNT interleaf layer with fiber bridging detected. This suggests that the CNT layer guided the crack, leading to a flat R-curve. Furthermore, crack propagation progresses exclusively in the CNT-rich region, corresponding to cohesive failure. [23]

Nasirmanesh et al. explored the effect of interleaving CNT sheet in a weave CFRP laminate on its impact damage resistance and interlaminar shear strength. The CNT sheet interleave in this study is placed in the midplane of the laminate as shown in figure 2.3.2.1. Low velocity impact test was carried out to determine the impact damage resistance. Results showed that the sample with CNT interleave received smaller damage area and intensity on the external surface, but larger internal damage area, as well as delamination and matrix cracks near the interleave. On the other hand,

the sample without CNT interleave produced the complete opposite results, with delamination and cracks near the surfaces. This result indicated that the interleaved CNT sheet has a buffering effect on the through-thickness impact damage from absorption of energy by the CNT layer. [21]

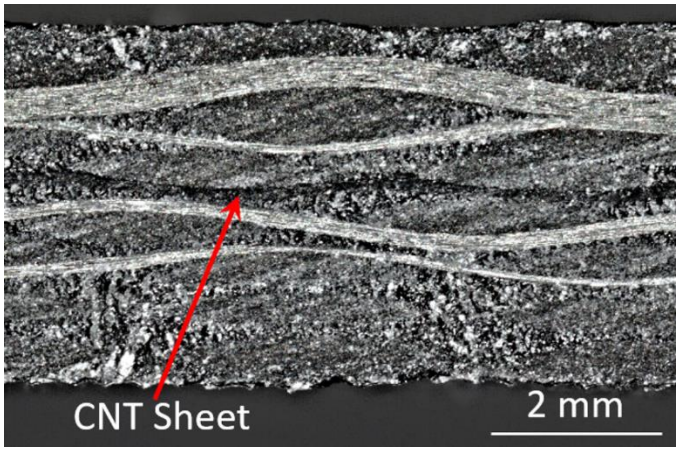

Figure 2.3.2.1 Through thickness microscopy image of weave CFRP laminate with CNT sheet interleave [21].

Short beam strength tests were then performed to determine the effect of CNT sheet interleave on interlaminar shear strength. The load-displacement curve for this test is shown in figure 2.3.2.2. This test was able to capture two dominating failure modes shown in figure 2.3.2.3: interlaminar shear failure and flexural tensile failure. The CFRP sample with CNT sheet interleave exhibited a slightly stiffer response compared to those without the interleave. The bigger difference is seen in the dominating failure mode between the different samples. The failure mode of the CNT sheet interleaved sample is dominated by flexural tensile failure, while samples without the interleave exhibited failure mode dominated by interlaminar shear. This result indicates that even a single CNT sheet interleave at the midplane can significantly

enhance the in-plane interfacial toughness under transverse load. Additionally, the single CNT sheet interleave is also capable of reducing the propensity for interlaminar shear failure effectively. [21]

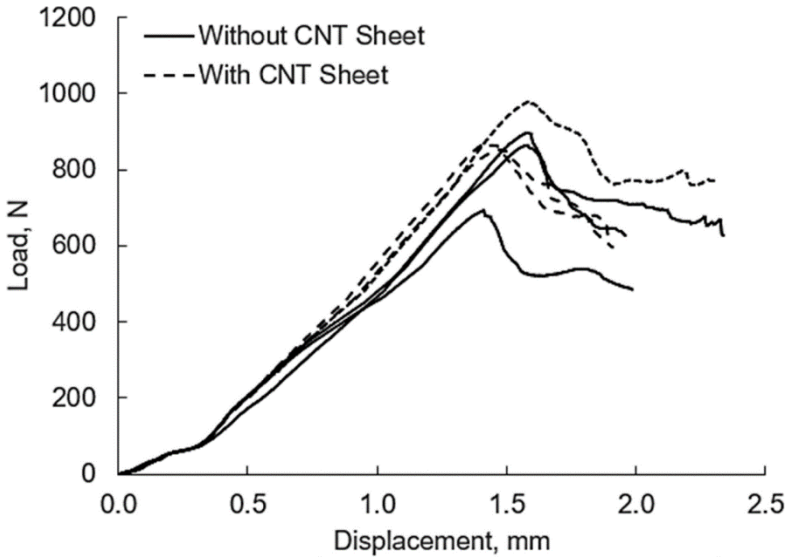

Figure 2.3.2.2 Load-displacement curve of short beam strength test [21].

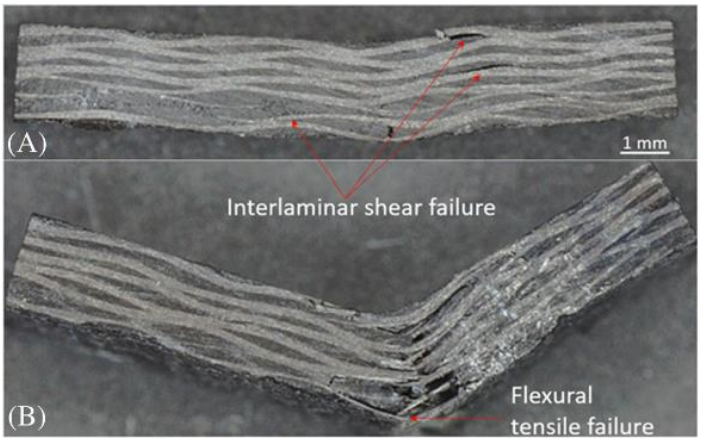

Figure 2.3.2.3 (A) Interlaminar shear failure and (B) flexural tensile failure from short beam strength test [21].

III. Experimental Procedure

Section 3.1 DCPD Preparation

Solid DCPD, obtained from Cymetech, is melted at 70°C and blended with 5-Ethylidene 2-Norbornene (ENB) at a weight ratio of 95:5 ENB:DCPD. The resulting mixture is degassed under full vacuum for 24 hours to prepare the stock DCPD solution. For experimental use, tributyl phosphite (TBP) and Grubbs second-generation catalyst (GC2) are incorporated as an inhibitor and catalyst, respectively, at a concentration of 100 ppm each. The mass formulation for these components is simplified as follows, providing the resin with approximately 30 minutes of working time before gelation occurs.

$$\mathrm{DCPD/ENB(grams)} = 1.557 * \mathrm{GC2(mg)}$$

$$\mathrm{TBP\ (\mu L)} = 0.3188 * \mathrm{GC2(mg)}$$

Section 3.2 Mass Loss Tests for DCPD

Mass loss tests are conducted using a TA instrument SDT Q600. Two specific tests are performed: Mass loss of DCPD during curing process and mass loss of fully cured DCPD. To prevent oxidation, a constant flow of argon gas is maintained at 50 mL/min for both tests. In the uncured DCPD test, the temperature is ramped up to 125°C, while in the cured DCPD test, it is set to 207°C, both at a rate of 10°C/min. The final temperature is maintained for 24 hours. Figure 3.2.1 shows the results of these mass loss tests.

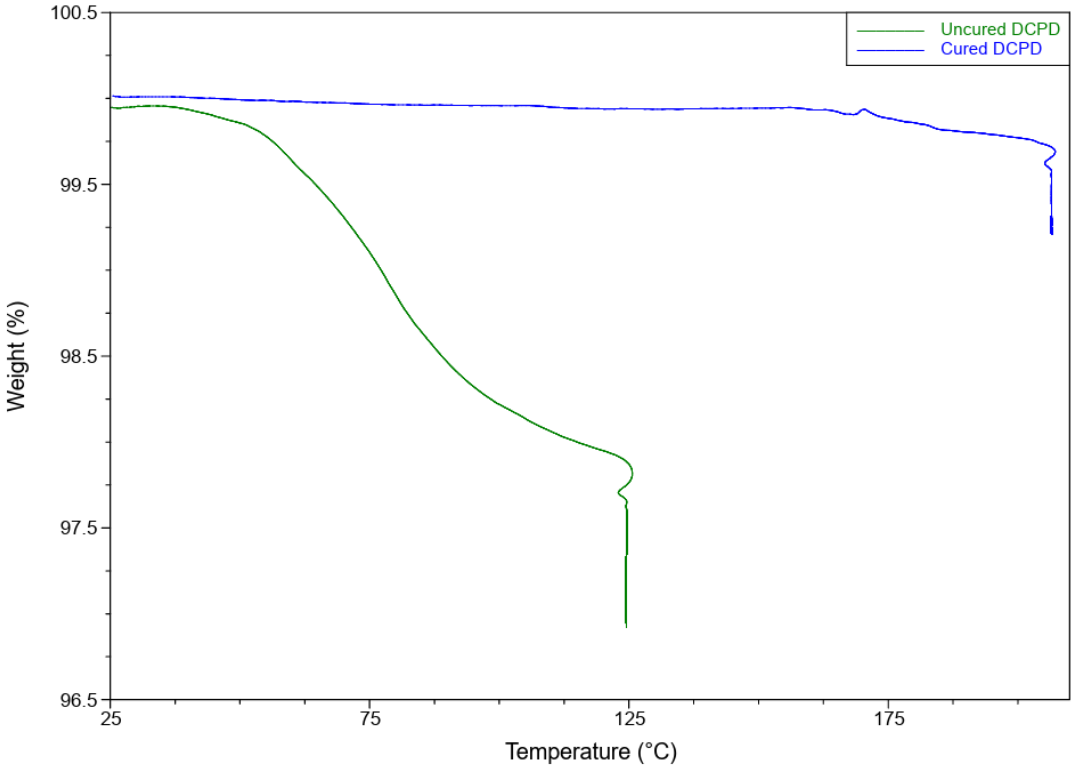

Figure 3.2.1 Total mass loss result for uncured and cured DCPD.

The results reveal significant mass loss during the curing process of DCPD, exceeding the acceptable value for space applications at approximately 4%. However, even at a much higher temperature, cured DCPD exhibits a mass loss of only 0.8%. This result shows that only cured DCPD is allowed in space and that any processes involving uncured DCPD must be executed on Earth.

Section 3.3 CFRP Tube Fabrication

To fabricate tubes, a bladder needs to be created to provide outward radial pressure while curing the tube. The bladder consists of a footlong super-soft latex rubber tube with 3/8” outer diameter connected to a hard nylon air tubing using a hose

worm clamp. The hard nylon side is linked to an air pump, and the end of the latex rubber side is sealed off by a rubber gasket to allow inflation as shown in figure 3.3.1.

Figure 3.3.1 Bladder for tube fabrication. (a) deflated, (b) inflated.

The CF tows used are T700 50C from Toray, and the CNT sheets are supplied by CrayTex. The CF tows are cut into 13-inch strips and the CNT sheets are cut into 0.5-inch x 13-inch ribbons. Two types of tubes are fabricated for this experiment: a tube consisting of a combination of CF tows and CNT sheets and a tube of only CF tows. In both cases, CF tows and CNT sheets are wetted with DCPD and laid up onto a 0.4-inch diameter mandrel covered by a release film.

For the combination tube, the layup configuration is structured in a way that ensures the inner and outer most layers of the tube consist of CNT sheets, while simulating how a strip containing both CF tow and CNT sheets fully cured CFRP strips shown in figure 3.3.2 would be laid up.

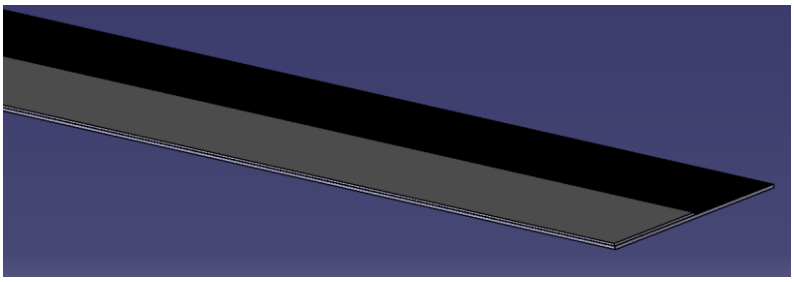

Figure 3.3.2 Potential cured CFRP strip.

The first few steps are shown in figure 3.3.3. First a CNT sheet ribbon is laid on the mandrel and a CF tow strip is placed on one edge as shown in (a) and (b). Then the next CNT sheet ribbon is laid next to the first CF tow as shown in (c) and another CF tow strip is placed on the edge of the second CNT sheet ribbon as shown in (d). This is repeated until 5 CF tow strips and CNT sheet ribbons are used, forming one layer of wet CF tow and CNT sheet. Consequent layers are flipped such that the CF tows are underneath the CNT sheets, ensuring the outermost layer is covered by CNT sheets. The final combination tubes are made up of 3 total layers of CF tows and CNT sheets.

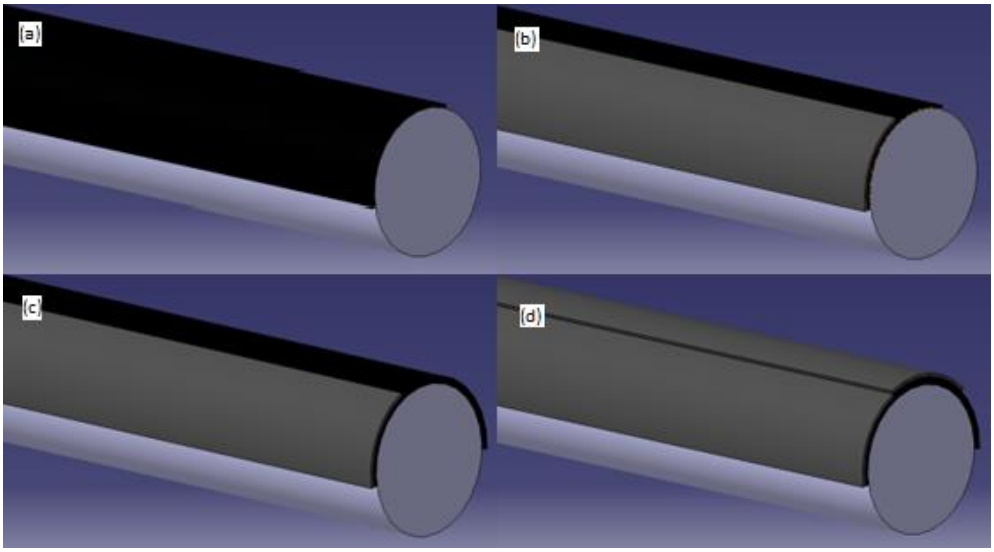

Figure 3.3.3 CF tows and CNT sheets layup sequence: (a) CNT sheet on barrel (b) CF tow lined up on one side of the first CNT sheet (c) second CNT sheet next to the first CF tow (d) CF tow placed on top of second CNT sheet next to first CF tow. Sequence repeated for 5 tows and CNT sheet to create the first layer.

As for the CF tow only tube, 40 strips of CF tows are used to fabricate an entire tube. Each layer consists of 5 strips of CF tows laid side by side all the way around the mandrel, resulting in a total of 8 layers of CF tows.

Once a tube is laid up on the mandrel, the release film allows the wet tube to be removed and transferred over to the bladder. The tube is then inserted inside a 0.5-inch barrel that is heated by a line heater to 150°C from the outside and lined with a layer of release film on the inside. The bladder is inflated to exert a force of 20 psi, pushing the tube against the barrel. This process is held for an hour before cooling the assembly in still air. The resulting fully cured tube is then removed and its edges are trimmed to produce a footlong as illustrated in figure 3.3.5.

Figure 3.3.4 Tube curing process setup. (b) Wrapped in line heater.

Figure 3.3.5 (a) Fully cured tube and (b) the tube cross section.

Section 3.4 CFRP Tube Flexural Strength Test

Unlike on Earth, where tensile or compressive strength often dominates, the key property for a support structure in space is its stiffness. To measure the stiffness of the CFRP tubes, a flexural strength test is conducted using an Instron 6800 universal testing system. The span length is adjusted to 16 times the diameter of the CFRP tube. The CF tow + CNT sheet tube has a diameter of 0.56 inches with the span length set to be 8.9 inches and the CF tow only tube has a diameter of 0.55 inches with the span length set to be 8.8 inches. In both cases the test is performed at a rate of 5mm/min. The test is recorded to better study the failure modes of the two types of CFRP tubes.

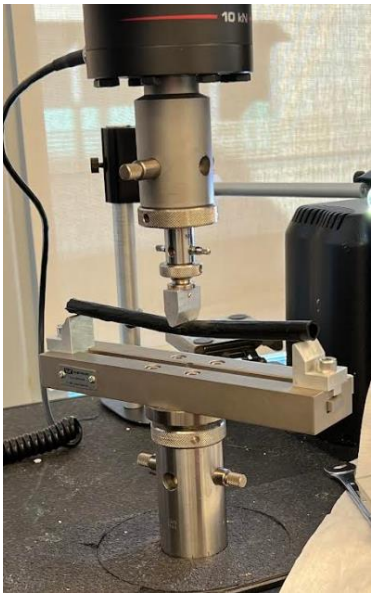

Figure 3.4.1 CFRP tube flexural strength test setup.

Section 3.5 CFRP Laminate Fabrication and Short Beam Shear Test

A potential solution to solve the mass loss issue involves manufacturing thin strips of CFRP using DCPD into rolls the traditional way on Earth. These rolls can then be transported to space for the fabrication of needed structures using adhesion methods other than DCPD. To evaluate the strength of adhesion between DCPD-cured CFRP strips, four different resins are tested: DCPD, JB Weld epoxy weld (JB), Devcon 2-ton epoxy (2TE), and Parbond 905 polyurethane.

Fully DCPD-cured strips of CF tow and CNT sheets like ones in figure 3.3.2 are to be bonded using the potential resins to test their adhesive strength. This is done by wetting CNT sheets and CF tows with DCPD and overlaying them to form the CF tow + CNT sheet strip. The strips are then hydraulic pressed under 3 tons of pressure for 30 minutes before they are baked in the oven at 150°C for an hour. Once the strips are

cured and cooled in still air, they are fused using the potential resins to create laminates for short beam shear testing.

Each laminate consists of 4 strips with the tows alternating as shown in figure 3.5.1. The laminates are then hydraulic pressed again and cured in the oven, producing a final thickness of 0.7mm. The laminates are finally trimmed into coupons to be used for the short beam shear testing. 3 coupons made from each resin are tested to compare their SBS strength. The SBS test is done on an Instron 6800 universal testing system. The span lengths are listed in table 3.5.1 and all tests are done at a rate of 1mm/min.

Figure 3.5.1 Laminate layup for short beam shear test.

Table 3.5.1 Dimensions of CFRP coupons for SBS testing

Resins	DCPD			JB Weld			2 Ton Epoxy			Parbond		
Thickness (mm)	0.6	0.6	0.48	0.73	0.67	0.8	0.74	0.74	0.64	0.68	0.7	0.65
Width (mm)	2.69	2.62	2.41	2.51	2.46	2.72	2.94	2.91	2.59	2.12	2.08	2.09
Length (mm)	3.26	3.26	3.26	3.26	3.26	3.26	3.31	3.31	3.31	3.31	3.31	3.31

Section 3.6 CFRP Tube Burnout for Fiber Volume Fraction

The fiber volume fraction stands as another important parameter to understand the properties of CFRP structures, relating directly to their mechanical performances. To measure the fiber volume fraction, the trimmed off portion of the CF tow + CNT sheet tube is fashioned into smaller tubes and are subjected to burnout. These small tubes are initially weighed and placed inside clean alumina crucibles, as shown in figure 3.6.1. The crucibles are then placed inside an oven at 565°C for 4 hours. Afterwards, the tubes are cooled in still air to room temperature before being reweighed. The weight losses are then used to calculate the fiber volume fraction using the densities of the materials used shown in table 3.6.1.

Figure 3.6.1 Burnout for FVF setup.

Table 3.6.1 Densities CF tow, CNT sheet, and DCPD

	CF tow	CNT sheet	DCPD
Density (g/mL)	1.8	0.13	1.02

IV. Experimental Results

Section 4.1 CFRP Tube Flexural Strength

The stiffnesses of the CF tow + CNT sheet tube and the CF only tow, characterized by the slope of the stress-strain curve, are compared through flexural strength test. The resulting stress-strain curve is shown in figure 4.1.1.

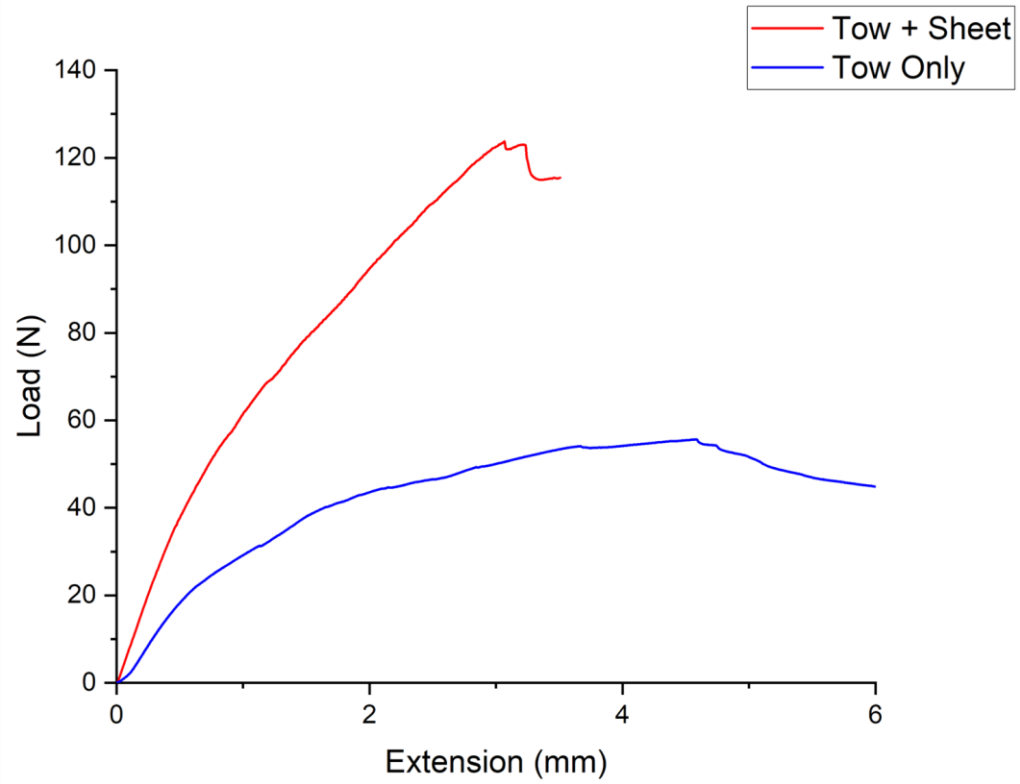

Figure 4.1.1 Stress-strain curve for CF tow only tube and CF tow + CNT sheet tube.

Figure 4.1.1 shows a notable increase in stiffness resulting from the incorporation of CNT sheets into the composition of the CFRP tube. The tube comprising solely of CF tow exhibits a stiffness of 32.40 N/mm whereas the inclusion of CNT sheets elevates the stiffness to about 70.24 N/mm, producing an improvement of over 115% while maintaining similar final tube dimensions.

In addition to figure 4.1.1, this difference in stiffness can also be seen throughout the flexural strength test process as shown in figure 4.1.2 and figure 4.1.3. In the tube consisting of only CF tow in figure 4.1.2, it is evident that the tube readily flattens under the applied load. The lower portion of the tube experiences minimal movement as the load cell presses down on the upper part, indicating the inherent weakness of CF tows in the transverse direction and resulting in a tube with low stiffness.

Conversely, the addition of CNT sheets significantly improves the tube's ability to withstand transverse loads as shown in figure 4.1.3. The deformation around the load cell is more pronounced, enabling the tube to maintain its hollow tubular shape everywhere else throughout the test. At the end of the test minimal flattening is observed and the deformation resembles more of a V-shaped bend rather than flattening. This shows the ability of a few layers of CNT sheets to reinforce the weak transverse strength of CF tows without significantly increasing the structure's thickness.

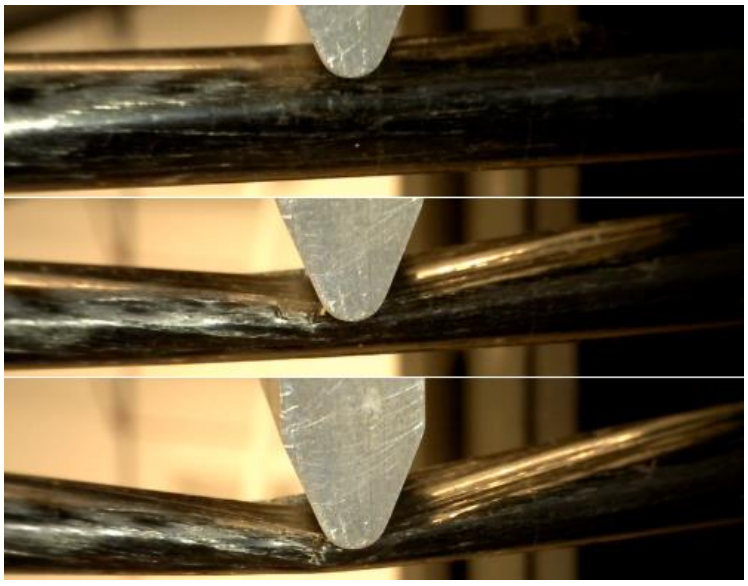

Figure 4.1.2 Flexural strength test transformation of the CF tow only tube.

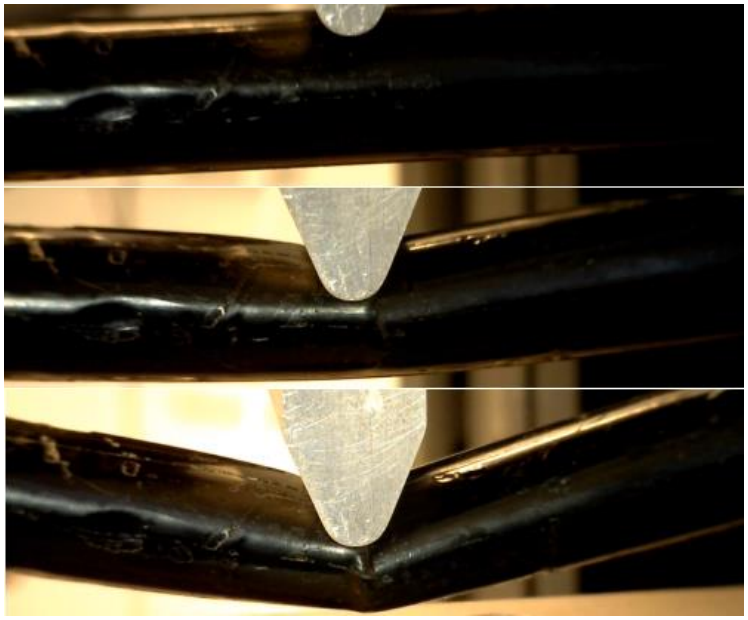

Figure 4.1.3 Flexural strength test transformation of the CF tow + CNT sheet tube.

One possible explanation for the improvement in stiffness through the addition of CNT sheet can be attributed to the random orientation of CNT within those sheets compared to the unidirectional fibers of the CF tows. The randomly oriented nanotubes contribute to strengthening the structure in all directions, although its impact is most pronounced in the transverse direction owing to the comparatively lower stiffness of unidirectional carbon fibers.

Section 4.2 Laminate SBS Strength

Figure 4.2.1 shows the stress-strain curve of the laminates that were fused with DCPD, JB Weld epoxy weld (JB), Devcon 2-ton epoxy (2TE), and Parbond 905 polyurethane. The SBS strengths of each adhesive are quantified by calculating the ratio of the maximum load to the cross-sectional area of the shear plane, as detailed in table 4.2.1.

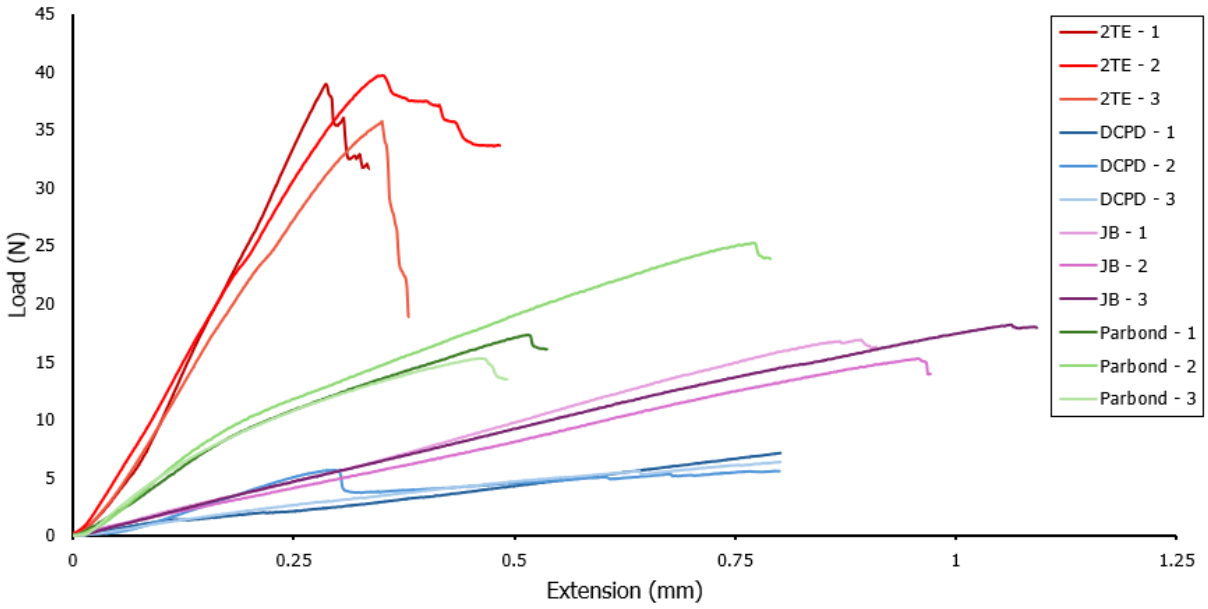

Figure 4.2.1 Stress-strain curve for laminates fused with DCPD, JB Weld epoxy weld (JB), Devcon 2-ton epoxy (2TE), and Parbond 905 polyurethane.

Table 4.2.1 SBS Strengths of laminate adhesives.

Adhesives	SBS Strength (MPa)
Devcon 2-ton epoxy	14.61 ± 1.32
DCPD	5.10 ± 1.57
JB Weld epoxy	6.85 ± 1.43
Parbond	10.65 ± 2.28

Both the stress strain curve as well as the table show that the 2TE exhibits the most promising strength among all tested adhesives, boasting an increase of nearly 200% compared to DCPD as the laminate adhesive. Following closely is the Parbond 905 polyurethane, demonstrating an improvement of about 100% over DCPD. Notably,

both the 2TE and Parbond samples were able to withstand the SBS test without delamination, exhibiting a failure mode similar to ductile yielding. On the other hand, both the DCPD and the JB weld epoxy initiate delamination shortly after the SBS test began, resulting in a delamination failure as shown in figure 4.2.2.

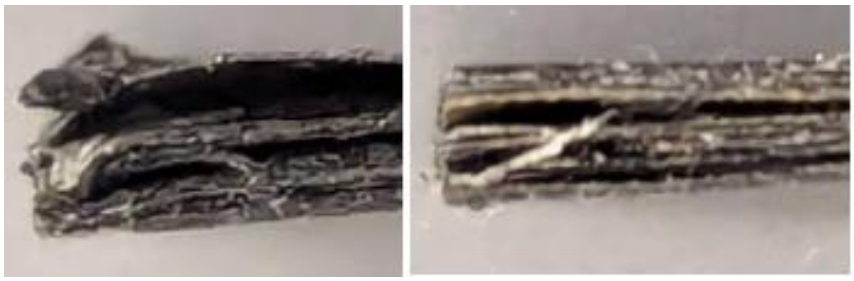

Figure 4.2.2 Delaminated samples from SBS testing.

Section 4.3 Fiber Volume Fraction

To calculate the fiber volume fraction, the weights of the samples are measured before and after the burnout process. Holding the oven at 565°C for 4 hours ensures the combustion of most of the DCPD while preserving all the CF tows and CNT sheets. This means the mass loss of the sample from the burnout corresponds to the mass of the DCPD present in the sample prior to the burnout. Based on the length of the baked sample tube, the mass of the CF tow in the sample can be computed, with the remaining mass constituting the CNT sheets. This results in an approximate composition of 80% CF tow by mass. Using this method, the FVF of 3 small tube samples are determined as shown in table 4.3.1.

Table 4.3.1 Measured values for burnout to determine FVF.

Samples	Mass before burnout (g)	Mass after burnout (g)	Carbon volume (mL)	DCPD volume (mL)	FVF (%)
1	0.731	0.153	0.293	0.567	34.1
2	0.552	0.179	0.340	0.366	48.1
3	0.676	0.170	0.325	0.495	39.6

The measured FVF appears unexpectedly low. Typically, a fiber volume fraction of at least 50% is considered desirable in a CFRP structure. A previous study in the lab suggested that the incorporation of CNT sheet should have significantly enhanced the FVF of the CFRP tube to upwards of 70 vol%[]. To gain a better understanding of the discrepancy in the FVF, an optical microscope is used to examine the cross-section of an unbaked tube.

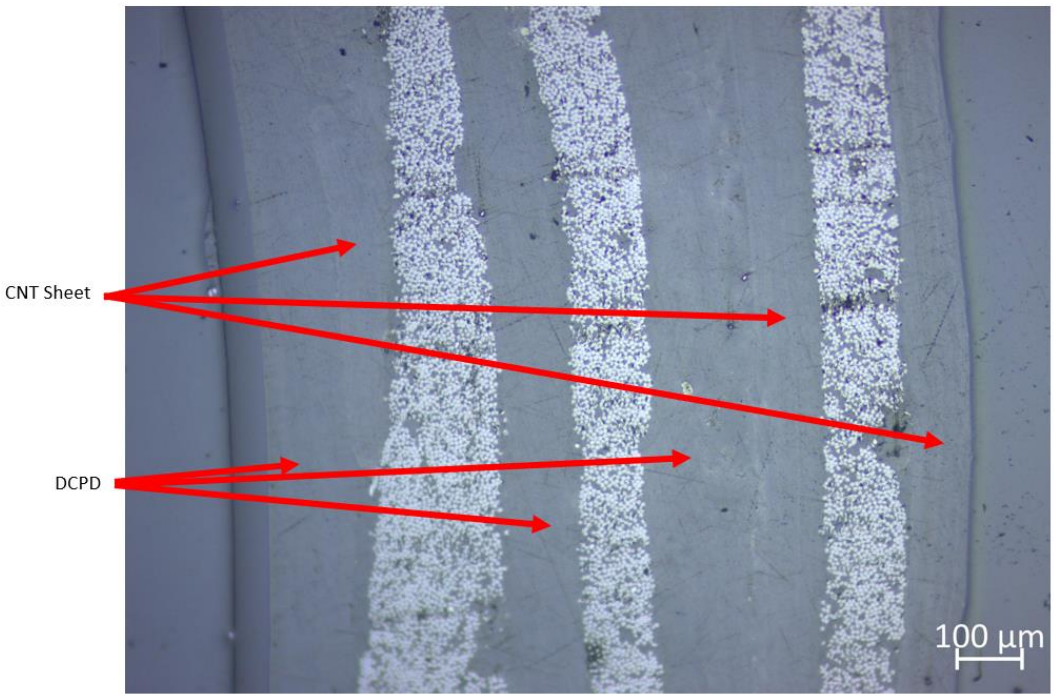

Figure 4.2.1 Microscopic view of CFRP tube cross-section.

Figure 4.2.1 shows the cross-section of the trimmed-off end of a fabricated CFRP tube. Upon closer inspection, thick layers of DCPD are discernible, trapped between the layers of CF tows and CNT sheets. The trapped DCPD significantly contributes to the deterioration in the FVF of the tube.

A possible explanation for this phenomenon may lie in the fabrication method used to produce the tubes. The static nature of the fabrication process, coupled with the relatively high aspect ratio of the tube allows DCPD to settle between the layers of CF tows and CNT sheets. In addition, CNT sheets exhibit low permeability, especially for the slightly viscous stage of DCPD used during fiber lay-up. As a result, the most efficient way for excess DCPD to escape is through the ends of the tube.

Possible solutions to mitigate the trapped DCPD involve employing dynamic fabrication methods for the tubes. One approach is by slowly increasing the pressure exerted by the bladder during fabrication, starting from the center of the tube towards both ends. The initial pressure would ensure that DCPD flows out both ends of the tube. Another, more interesting alternate fabrication method is by extruding or pultruding the tube out of the barrel. In this concept, the fabrication setup is static while the tube is physically pushed or pulled out of the barrel, leaving the resin behind due to the pressure applied by the bladder. Notably, this method would also enable continuous fabrication of tube that can be cut into desirable lengths.

Despite the low FVF of the produced CFRP tube, its mechanical properties still surpass those of the CF tows only tube. By improving the FVF, it is anticipated that these properties will experience significant improvement.

V. Summary

Sending fully manufactured CFRP support structures from Earth surface to orbit continues to be a challenge in both cost and efficiency. To combat this, DARPA started NOM4D, a project that aims to enable the ability to manufacture such structures in orbital facilities. This thesis assists the project by exploring different configurations of carbon fiber layups with DCPD to produce a high stiffness and FVF tubular structure with low mass loss as proof-of-viability for space applications.

TML test was performed to confirm the NASA-implemented rule which limits total mass loss of less than 1% for materials in space. The curing process of DCPD resulted in a mass loss of 4%, but once cured, this value drops to 0.8%. This proves materials must be pre-processed on Earth such that space manufacturing only involves cured DCPD.

From the result of the TML test, other means of adhesion to bond fully cured CFRP strips to form a structure. DCPD, JB Weld epoxy weld (JB), Devcon 2-ton epoxy (2TE), and Parbond 905 polyurethane are used to fabricate coupons of CF tows and CNT sheets to be used for SBS test. The highest SBS strength was seen from the coupons bonded with the 2-ton epoxy followed by the Parbond epoxy, as these coupons remained intact at the end of the test. On the other hand, using DCPD and the JB weld epoxy to bond the coupons resulted in weak SBS strength and delamination was observed from the SBS test.

Two types of tubes are fabricated in this project: a CF tow only tube and a CF tow + CNT sheet tube. The flexural strength test showed that the presence of CNT

sheet within the tube enhanced its stiffness by over 115% compared to the tube consisting only of unidirectional CF tows. The randomly oriented nanotubes in the CNT sheets are believed to be responsible for this improvement, increasing the tube's strength by distributing loads more efficiently.

Burnout is performed on the tube containing the CNT sheet to determine its fiber volume fraction. After burning off the all the resin in the tube, the FVF is calculated from the remaining mass. The test resulted in a fiber content in the ballpark of 40 vol%, which is far lower than expected. To better understand this number, the cross section of the fabricated tube is observed under an optical microscope, showing large amounts of DCPD within the layers of CF tows and CNT sheets. It is believed that changing the fabrication method to one that is more dynamic, such as extrusion or pultrusion, would allow DCPD to be drained more efficiently, thus increasing FVF closer to the expected value.

VI. Future Work

Section 6.1 Finishing Phase 1

New fabrication procedures need to be explored to create tubes with less trapped DCPD in its layers. Possible solutions would be to use a slowly expanding bladder or pultruding the tube using a machine. Once this is achieved, the configuration of the tubes would also need to be changed, because with less resin in between the layers the thickness of the tube would be much smaller. This allows more layers to be added to meet the 1mm thickness requirement and more combinations of CF tows and CNT sheets layers to be experimented to determine which can produce the maximum stiffness and FVF.

Since adhesives strong enough to bond the DCPD-cured CFRP ribbons have been determined, the space qualifications need to be tested. TML test needs to be done on Devcon 2-ton epoxy (2TE) and Parbond 905 polyurethane to confirm that they are viable for space applications. Depending on the results, new means of adhesion may need to be explored to find a viable solution to only using cured DCPD in space.

Section 6.2 Future of the Project

Moving forward with the next phase of the project, the tube is to be stepped up to 2-inch diameter from the 0.5-inch diameter tubes in this paper. New procedures would be needed to fabricate this large tube since it would require 4 times as much materials as the 0.5-inch tube, thus complicating the time constraint of the uncured DCPD. This opens the possibility of using the fully DCPD cured ribbons of CF tows and CNT sheets along with adhesives explored in this paper to fabricate the tubes.

Along with fabricating larger tubes, phase 2 also entails fabricating the tubes with a machine continuously. In the case of this project, the tubes are to be pultruded through a pultrusion machine. To do this a pultrusion machine needs to be built that is capable of taking multiple reels of cured CFRP strip with adhesive applied on it and heated to cure under pressure in a barrel. As of right now, the pultrusion machine is partly built as shown in figure 6.2.1.

Figure 6.2.1 Partially built pultrusion machine to fabricate tubes.

So far, the machine is to function by pulling tubes and CFRP strips along the mandrel and through the barrel using rollers. The rollers are powered by NEMA 23 stepper motors with speed controlled by an Arduino processor. This partially built machine serves as a skeleton that can be modified and tailored to needs that may arise in the future. For phase 2, such modifications include upgrading the size of the mandrel, barrel, and rollers to fit the 2-inch diameter requirement as well as applying

the bladder to apply outward pressure from inside the tube. However, this may prove difficult as the tube would only be supported by the bladder once inside the barrel. Ideally, the bladder wouldn't be inflated throughout the entire process as it may impede the movement of the tube. Instead, the bladder should be pulsed using an air piston, allowing the tube to move more efficiently with less friction. A schematic of the would-be finished pultrusion machine is shown in figure 6.2.2.

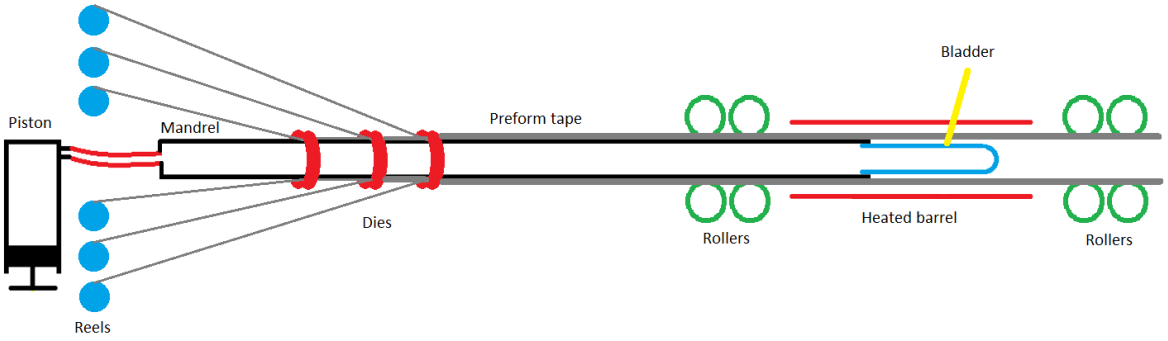

Figure 6.2.2 Schematic of significant parts in a completed pultrusion machine.

VII. References

[1] Sun B, Xue C, Shang W, An M, Zhao H, Zhang H. The performance characterization of carbon fiber–reinforced plastic for space applications. Journal of Reinforced Plastics and Composites. 2023;42(15-16):844-853.

[2] G.G. Reibaldi. Thermomechanical behaviour of CFRP tubes for space structures. Acta Astronautica. Volume 12, Issue 5. 1985. Pages 323-333.

[3] Composites applications for space. (n.d.). https://www.nasampe.org/page/CompositesApplicationsforSpace.

[4] Xin W, Severino J, Venkert A, Yu H, Knorr D, Yang J-M, Carlson L, Hicks R, De Rosa I. Fabrication and Characterization of Solid Composite Yarns from Carbon Nanotubes and Poly(dicyclopentadiene). Nanomaterials. 2020; 10(4):717.

[5] Cheng F, Hu Y, Yuan B, Hu X, Huang Z. Transverse and longitudinal flexural properties of unidirectional carbon fiber composites interleaved with hierarchical Aramid pulp micro/nano-fibers. Composites Part B: Engineering Volume 188. 2020.

[6] Hayne D, Singleton M, Patterson B, Wickramasingha Y, Sietins J, Knorr D, Stojcevski F, Henderson L. Assessing the properties of Poly(dicyclopentadiene) reinforced with discontinuous carbon fibers. Composites Part A: Applied Science and Manufacturing. Volume 155. 2022.

[7] Yang G, Lee J. Curing Kinetics and Mechanical Properties of endo-Dicyclopentadiene Synthesized Using Different Grubbs' Catalysts. Industrial & Engineering Chemistry Research 2014 53 (8), 3001-3011.

[8] L. Zhu, N. Li, P.R.N. Childs. Light-weighting in aerospace component and system design. Propulsion and Power Research Volume 7, Issue 2. 2018. Pages 103-119.

[9] Bielawski C, Grubbs R. Living ring-opening metathesis polymerization. Progress in Polymer Science, Volume 32, Issue 1. 2007. Pages 1-29.

[10] Sutthasupa S, Shiotsuki M & Sanda F. Recent advances in ring-opening metathesis polymerization, and application to synthesis of functional materials. Polym J 42, 905–915 (2010).

[11] Robertson I, Pruitt E, and Moore J. Frontal Ring-Opening Metathesis Polymerization of Exo-Dicyclopentadiene for Low Catalyst Loadings. ACS Macro Letters 2016 5 (5), 593-596.

[12] Mariani A, Fiori S, Chekanov Y, and Pojman J. Frontal Ring-Opening Metathesis Polymerization of Dicyclopentadiene. Macromolecules 2001 34 (19), 6539-6541.

[13] Li Q, Shen H, Liu C, Wang C, Zhu L, Chen S. Advances in frontal polymerization strategy: From fundamentals to applications. Progress in Polymer Science, Volume 127. 2022.

[14] Goli E, Robertson I, Geubelle P, and Moore J. Frontal Polymerization of Dicyclopentadiene: A Numerical Study. The Journal of Physical Chemistry B 2018 122 (16), 4583-4591.

[15] Robertson I, Dean L, Rudebusch G, Sottos N, White S, and Moore J. Alkyl Phosphite Inhibitors for Frontal Ring-Opening Metathesis Polymerization Greatly Increase Pot Life. ACS Macro Letters 2017 6 (6), 609-612.

[16] Bussiba A, Gilad I, Lugassi S, David S, Bortman J, Yosibash Z. Mechanical Response and Fracture of Pultruded Carbon Fiber/Epoxy in Various Modes of Loading. Crystals. 2022; 12(6):850.

[17] Sebaey T, Blanco N, Costa J, Lopes C. Characterization of crack propagation in mode I delamination of multidirectional CFRP laminates. Composites Science and Technology, Volume 72, Issue 11. 2012. Pages 1251-1256.

[18] Nardelli M, Fattebert J, Orlikowski D, Roland C, Zhao Q, Bernholc J. Mechanical properties, defects and electronic behavior of carbon nanotubes. Carbon, Volume 38, Issues 11–12. 2000. Pages 1703-1711.

[19] Han W, Zhou J, Shi Q. Research progress on enhancement mechanism and mechanical properties of FRP composites reinforced with graphene and carbon nanotubes. Alexandria Engineering Journal, Volume 64. 2023. Pages 541-579.

[20] Saadatyar S, Beheshty MH, Sahraeian R. Mechanical properties of multiwall carbon nanotubes/unidirectional carbon fiber-reinforced epoxy hybrid

nanocomposites in transverse and longitudinal fiber directions. Polymers and Polymer Composites. 2021.

[21] Nasirmanesh A, Singh A, Villaflor D, Blandford B. Effects of midplane carbon nanotube sheet interleave on the strength and impact damage resistance of carbon fiber reinforced polymer composites. Polym. Compos. 2022, 43(5), 3085.

[22] Zhu M, Gorbatikh L, Lomov S. An incremental-onset model for fatigue delamination propagation in composite laminates. Composites Science and Technology, Volume 200. 2020.

[23] Ou Y, González C, Vilatela J. Interlaminar toughening in structural carbon fiber/epoxy composites interleaved with carbon nanotube veils. Composites Part A: Applied Science and Manufacturing, Volume 124. 2019.

[24] Maruyama T. Chapter 6 - Carbon nanotubes. In Micro and Nano Technologies. Handbook of Carbon-Based Nanomaterials. Elsevier. 2021. Pages 299-319.

[25] Yu, M. Fundamental Mechanical Properties of Carbon Nanotubes: Current Understanding and the Related Experimental Studies. ASME. J. Eng. Mater. Technol. July 2004; 126(3): 271–278.

[26] Shirasu K, Yamamoto G, Nelias D, Hashida T. Mechanical and Fracture Properties of Carbon Nanotubes. InTech. (2018).